
Live Constrained Deep Learning Models Optimize Unmanned Underwater Vehicle Control Systems

Anonymous Author(s)

Affiliation

Address

email

Abstract

1 Unmanned Underwater Vehicles (UUVs) are critical for a variety of societally-
2 important missions such as ocean monitoring, but mission times are constrained by
3 the compute and power constraints on UUVs. We develop a constrained inverse
4 search model that leverages kinematics-to-thrust and kinematics-to-power neural
5 networks to find a set of optimal fin kinematics with the multi-objective goal of
6 reaching a target thrust under power constraints while creating a smooth kine-
7 matics transition between flapping cycles. We demonstrate how a control system
8 integrating this model can make online, cycle-to-cycle adjustments to prioritize
9 different system objectives. Implementing inverse search can allow for a reduction
10 in power consumption of 66% for a 0.1 N tradeoff in thrust propulsion, while
11 rigidity improvements can further reduce thrust loss by 74%, and reduce power
12 consumption by 37%.

13 **1 Introduction**

14 Unmanned underwater vehicles (UUVs) have a variety of societal applications including mapping
15 the sea floors (1; 2), inspecting underwater pipelines (3; 4), and monitoring water quality (5; 6; 7;
16 8; 9; 10; 11; 12). These tasks are critical to proactively protecting against oil spills, conserving
17 limited water resources, and mitigating the environmental damages perpetuated by human activities to
18 aquatic environments. Among various options for UUV systems, bio-inspired robotics offer potential
19 advantages for these missions. Studies have demonstrated that animals swim at an optimal Strouhal
20 number for power efficiency (13; 14; 15), which flapping fins can imitate for high maneuverability
21 at low speeds (16; 17) while being less polluting and more non-intrusive in aquatic environments
22 compared to other systems (18; 10; 19), leading many UUVs to be based on bio-inspired designs
23 (8; 18; 10; 12).

24 Previous studies have explored the effects that varying material, flexibility, and shape alongside
25 kinematic inputs have on a flapping fin’s thrust output and power efficiency to better replicate fish
26 hydrodynamics (20; 21; 22; 23; 24) and inform design (25; 26; 23). Various approaches including
27 high-fidelity computational fluid dynamics (CFD) simulations (27) and using machine learning to
28 develop surrogate models (28; 29) have provided the ability to predict a certain thrust output of a
29 single gait, but simulations are computationally expensive and impractical in real-world environments
30 (30; 31).

31 Critically, many important real-time water sampling missions on bio-inspired UUV systems often
32 are impractical due to power and compute constraints that limit the UUV’s mission duration, forcing
33 researchers to select only the most critical regions for their monitoring, leaving certain regions
34 vulnerable (32). We propose a computationally-constrained and efficient inverse-search method
35 that searches possible gaits to make real-time movement adjustments to optimize for mission dura-
36 tion, efficiency, and propulsion. Inverse search methods are challenging for compute-constrained

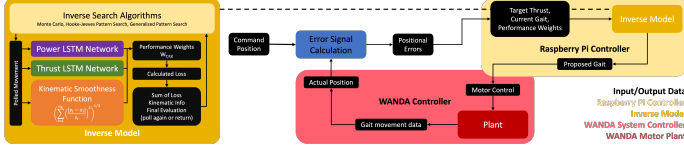


Figure 1: Visualization of the integrated inverse model on the control system.

37 autonomous systems. Typically, they are only implemented offline as it requires invoking a forward
 38 model multiple times (33; 34). Other approaches, such as direct inverse models comprised of neural
 39 networks (35; 36; 37; 38) are fast, but are not able to make live cycle-by-cycle optimizations for
 40 various metrics such as propulsive efficiency, which could drastically shorten mission times and make
 41 missions possible.

42 In this work, we demonstrate that a generalizable search-based (39) inverse model optimizing thrust,
 43 kinematics smoothness, and power consumption each cycle can meet compute and power constraints
 44 in live time through benchmarking while significantly improving the efficiency of selected kinematics
 45 without a tradeoff of thrust generation by analyzing various combinations of weights to determine
 46 optimizations for various missions, extending maximum mission times on fin-based system.

47 2 Methods

48 Displayed in Figure 1, the inverse model operates each cycle based on three inputs from the PID
 49 controller (40): desired thrust, current gait, and optimization weights to output a proposed gait. This
 50 proposed gait given to an onboard microcontroller, which switches to the new gait after a cycle. The
 51 cycle repeats, and an error signal calculation updates the position to request the next desired thrust.

52 A singular gait is comprised of four kinematic parameters: stroke phase offset (δ), stroke amplitude
 53 (Φ), pitch amplitude (Θ), and flapping frequency (f). For each unique gait, we collected experimental
 54 data on the forces generated in the x, y and z axes, current drawn by each motor, and circuit voltage for
 55 the different fin gaits (41). Calibrated potentiometers (TT Electronics P260) measure the stroke and
 56 pitch angles over time. Load cells (Interface 3A60A) measure the generated forces (42), and current
 57 and voltage sensors provide information to compute the power. The range of gaits is constrained to
 58 parameter values that are physically achievable given a frequency. At higher frequencies, the fins are
 59 physically unable to reach certain amplitudes: the maximum stroke and pitch given any frequency is
 60 calculated with $\Phi = 68 * f^{-1.4}$ and $\Theta = 50 * f^{-1}$ respectively, a best fit to empirical data collected
 61 on achievable angles at specified stroke frequencies.

62 This range covers 864 unique gaits, collected three times for three unique fins of varying rigidity
 63 ranging from most to least flexible: rigid, PDMS 1:10, and PDMS 1:20. This data trains six individual
 64 forward Long Short Term Memory (LSTM) models that predicts either the thrust generated or power
 65 consumed based on a given gait. All models were implemented in TensorFlow and benchmarked
 66 for run-time speed on a Raspberry Pi 4B. The LSTM was able to minimize error compared to other
 67 fine-tuned models tested including a linear regression, quartic regression, MLP, CNN, and DNN
 68 further detailed in (41). Across a range of 2.4 N and 8.9 W, the rigid fin model has an error of 0.0002
 69 N and 0.0037 W, PDMS 1:10 of 0.0186 N and 0.0084 W, and PDMS 1:20 of 0.0041 N and 0.0105 W.

70 Shown in Figure 1, the inverse model communicates with the control system to understand the current
 71 state and search for the next gait. The controller feeds the inverse model three metrics: the current gait,
 72 the desired thrust, and a set of performance metric weights (for propulsion, kinematics smoothness,
 73 and power) that guide the search algorithm. The inverse model samples possible gaits and uses a
 74 multi-objective loss function integrated into a Generalized Pattern Search (GPS) method (39) to find
 75 a gait that is as close as possible to the desired thrust outcome and meets the priorities weighted. This
 76 search algorithm invokes both forward gait-to-thrust and gait-to-power models hundreds of times in a
 77 single search to accurately predict the thrust and power outcomes of a sampled gait. The finalized
 78 gait is sent to the control system. The error signal calculation updates the current position to find the
 79 next desired thrust for the inverse model, and another cycle will begin.

80 As the maximum flapping frequency of any gait is 2Hz, the inverse model is required to generate
 81 a gait within 0.45 seconds when accounting for time communicating with the control system and

82 calculating positional error. To meet compute and power constraints on the control system, the
 83 inverse model is benchmarked on a Raspberry Pi 4 Model B, and forward gait-to-thrust/power models
 84 are shrunk and compressed to meet size and runtime constraints. In selecting optimal set of fin
 85 kinematics, preference is given to high thrust, low power, and smooth kinematics using weights that
 86 sum to one: $w_T + w_P + w_K = 1$. w_T is the weight on thrust, w_P is the weight on power, and w_K is
 87 the weight on kinematics smoothness. These modify the loss values for thrust, power, and kinematics
 88 smoothness, and the system adjusts the weights based on current mission priorities each cycle.

89 3 Experimental results

90 Three separate inverse control models are developed using the characteristics of each material's
 91 forward gait-to-thrust and gait-to-power neural networks. All three models meet benchmarking
 92 requirements when tested on a Raspberry Pi Model 4B: the rigid inverse control model returns a result
 93 after $0.208252s$ on average, the PDMS 1:10 inverse control model returns a result after $0.201874s$
 94 on average, and the PDMS 1:20 inverse control model returns a result after $0.191625s$ on average.

95 To evaluate the inverse models on realistic thrust requests, we generated requests using a PID
 96 controller for vehicle position in the Simulink environment (43), with the results in Figure 2. The
 97 controller outputs a target thrust to control a simulated thrust-to-position plant that models the UUV
 98 based on the translational equations of motion for a rigid body. We simulate UUV movement to 100
 99 randomly generated positions between 0 and 10m. For each location, the controller commands a
 100 thrust between -1.2N and 1.2N for 15 flapping cycles to reach and then remain at the position. The
 101 PID controller-generated thrusts enable the simulated UUV to accurately track changes to the target
 102 position. Small positional changes are included to simulate the start and stop conditions of the UUV:
 103 intermediary movement is less reliant on the inverse model since the UUV thrust is held constant at
 104 the maximum or minimum value. When compared with other inverse search approaches based on the
 105 Monte Carlo (44; 45) and Hooke-Jeeves Pattern Search (46) algorithms, the GPS method searches
 106 promising points in situations where the algorithm is potentially trapped in a local minimum during
 107 polling failure. These additional searches enable the GPS inverse model to maintain a lower loss.

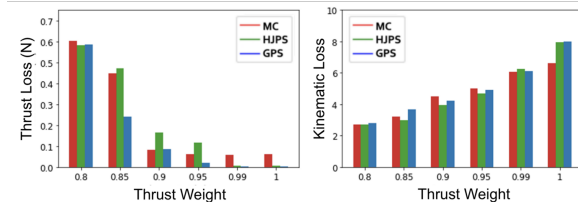


Figure 2: Inverse model performance for simulated data, measured by thrust accuracy loss (left) and kinematic smoothness loss (right). Note $w_k = 1 - w_t$.

108 To test the performance gains provided from the inverse control model with three optimization metrics
 109 T , K , and P , we repeat this set of thrust requests for all combinations of optimization weights with
 110 a 0.05 difference. Figure 3 displays many runs of the test with varying sets of weights. Power loss
 111 and kinematics loss exhibit similar behaviors; weighting either against thrust has similar behavior at
 112 high weights. The most important areas of each triangle are where $w_T > 0.7$, where a significant
 113 observable trade off between thrust and power/kinematics smoothness exists. This is consistent what
 114 we would expect; as the GPS algorithm is basing its search off of a requested thrust from the control
 115 system, any algorithm that assigns a low weight to w_T will result in convergence to the same gaits.

116 When $w_T > 0.8$, L_T is generally below 0.2 N for all materials. While improvements can be
 117 made to minimize thrust loss to 0.06 N as (w_T, w_K, w_P) approaches $(1, 0, 0)$, a generally efficient
 118 combination around $(0.8, 0, 0.2)$ can reduce the power consumption of the gaits used by more
 119 than two thirds; for a 0.1 N trade off in thrust loss, gait power decreases from a prior 4.2 W to
 120 approximately 1.5 W, significantly reducing the power consumption in a total range of 0-1.2 N and
 121 0-7.9 W. These various combinations demonstrate optimal weights for certain tasks, such as rapid
 122 acceleration, efficient movement, and energy-efficient station-keeping.

123 While the profile of each set of optimization weights relative to its neighbors is similar, the flexible
 124 PDMS 1:10 and 1:20 designs have lower thrust losses and lower power requirements compared to the

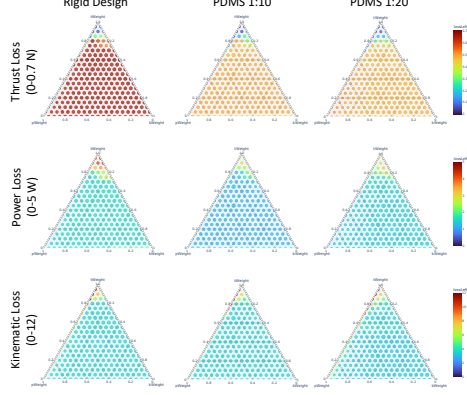


Figure 3: Analysis of different weight sets. Red indicates high loss, blue indicates low loss (47).

125 rigid fin. While the rigid fin averages a thrust loss of 0.7 N and a power of 1.5 W, the flexible designs
126 average a thrust loss of around 0.5 N with a power loss of around 1.3W. The PDMS 1:10 design is
127 the most effective at minimizing thrust and power loss simultaneously.

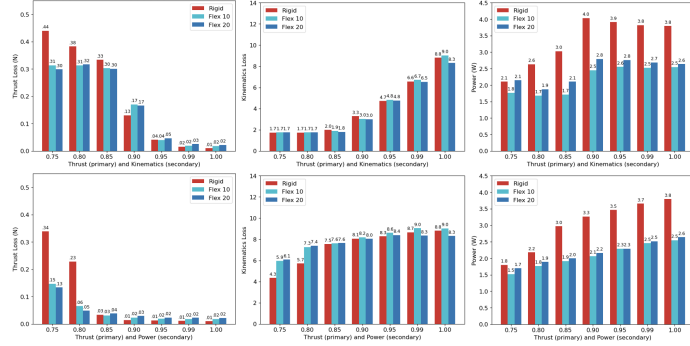


Figure 4: A grid of L_T , L_K , and L_P in columns for W_T trading off with W_K (row 1) or W_P (row 2).

128 In the results in Figure 4, L_K improves across the board for all three fin materials. The flexible
129 PDMS materials both continue to outperform the rigid material in minimizing both thrust and power
130 loss. At (0.8, 0.0, 0.2), the flexible fins cut L_T by an average of 74%. Although the flexible fins
131 reduce L_T for values where $w_T < 0.8$, it no longer halves the loss when trading off w_T with w_K .
132 The flexible design only reduces L_T by around a quarter, but reduces L_P further. At values where
133 $w_T > 0.85$, the flexible fins improve upon the power loss of the rigid fins by an average of 37%.

134 4 Conclusion

135 This study uses deep learning to optimize the propulsion and power consumption gaits to yield the
136 same propulsive outcome. We develop and test an inverse search model that utilizes two forward
137 LSTM models with an accuracy of 0.0076 N and 0.0072 W. The inverse search model, benchmarked
138 within necessary time constraints, can optimize between thrust propulsion, kinematics smoothness,
139 and efficiency cycle by cycle. By default, use of the inverse model reduces power consumed for any
140 requested thrust by an average of 66%, or 3 W. We can conclude that both flexible PDMS 1:10 and
141 1:20 materials are more efficient and propulsive compared to the rigid fin, with the PDMS 1:10 fin
142 being the most efficient and propulsive overall; with the same gait, the 1:10 mixture improved thrust
143 outcomes by upwards of 74% and power outcomes by upwards of 37%. Improvements from inverse
144 search are amplified with the 1:10 material. For any material, inverse search methods improve thrust
145 outcome by 29% and reduce power consumption by 33% simultaneously using a default optimization
146 set of (0.8, 0.0, 0.2). The system can then further adjust to optimize for efficiency, extending mission
147 times, or propulsion, increasing acceleration after every cycle, allowing for more flexible missions.

148 **References**

- 149 [1] E. C. Gezer, L. Zhao, J. Beason, and M. Zhou, "Towards seafloor mapping using an affordable
150 micro-UUV," in *OCEANS 2021: San Diego – Porto*, (San Diego, CA, USA), pp. 1–5, IEEE,
151 Sept. 2021.
- 152 [2] F. Heubach and M. Seto, "Generation of Augmented Bathymetry to Aid Development of Terrain-
153 Aided Autonomous Underwater Vehicle Localization and Navigation Approaches," in *OCEANS
154 2021: San Diego – Porto*, (San Diego, CA, USA), pp. 1–6, IEEE, Sept. 2021.
- 155 [3] I.-C. Sang and W. R. Norris, "An Autonomous Underwater Vehicle Simulation With Fuzzy
156 Sensor Fusion for Pipeline Inspection," *IEEE Sensors Journal*, vol. 23, pp. 8941–8951, Apr.
157 2023.
- 158 [4] J. He, J. Wen, S. Xiao, and J. Yang, "Multi-AUV Inspection for Process Monitoring of Under-
159 water Oil Transportation," *IEEE/CAA Journal of Automatica Sinica*, vol. 10, pp. 828–830, Mar.
160 2023.
- 161 [5] D. Y. Kwon, J. Kim, S. Park, and S. Hong, "Advancements of remote data acquisition and
162 processing in unmanned vehicle technologies for water quality monitoring: An extensive review,"
163 *Chemosphere*, vol. 343, p. 140198, Dec. 2023.
- 164 [6] S. Yang, P. Liu, and T. H. Lim, "IoT-based underwater robotics for water quality monitoring in
165 aquaculture: A survey," 2023.
- 166 [7] I. Y. Amran, K. Isa, H. A. Kadir, R. Ambar, N. S. Ibrahim, A. A. A. Kadir, and M. H. A.
167 Mangshor, "Development of Autonomous Underwater Vehicle for Water Quality Measurement
168 Application," in *Proceedings of the 11th National Technical Seminar on Unmanned System
169 Technology 2019* (Z. Md Zain, H. Ahmad, D. Pebrianti, M. Mustafa, N. R. H. Abdullah,
170 R. Samad, and M. Mat Noh, eds.), (Singapore), pp. 139–161, Springer Nature, 2021.
- 171 [8] C. Kai, Z. Weiwei, and D. Lu, "Research on Mobile Water Quality Monitoring System Based on
172 Underwater Bionic Robot Fish Platform," in *2020 IEEE International Conference on Advances
173 in Electrical Engineering and Computer Applications(AECA)*, (Dalian, China), pp. 457–461,
174 IEEE, Aug. 2020.
- 175 [9] Y. Li, R. Liu, and S. Liu, "The Design of an Autonomous Underwater Vehicle for Water Quality
176 Monitoring," *IOP Conference Series: Materials Science and Engineering*, vol. 301, p. 012137,
177 Jan. 2018. Publisher: IOP Publishing.
- 178 [10] D. Karimanzira, M. Jacobi, T. Pfuetzenreuter, T. Rauschenbach, M. Eichhorn, R. Taubert, and
179 C. Ament, "First testing of an AUV mission planning and guidance system for water quality
180 monitoring and fish behavior observation in net cage fish farming," *Information Processing in
181 Agriculture*, vol. 1, pp. 131–140, Dec. 2014.
- 182 [11] M. Eichhorn, R. Taubert, C. Ament, M. Jacobi, and T. Pfuetzenreuter, "Modular AUV system
183 for Sea Water Quality Monitoring and Management," in *2013 MTS/IEEE OCEANS - Bergen*,
184 (Bergen, Norway), pp. 1–7, IEEE, June 2013.
- 185 [12] H. Yu, A. Shen, and L. Peng, "A new Autonomous Underwater Robotic Fish designed for water
186 quality monitoring," *Identification and Control*, 2012.
- 187 [13] M. H. Masud, M. La Mantia, and P. Dabnichki, "Estimate of Strouhal and Reynolds numbers
188 for swimming penguins," *Journal of Avian Biology*, vol. 2022, no. 2, p. e02886, 2022. _eprint:
189 <https://onlinelibrary.wiley.com/doi/pdf/10.1111/jav.02886>.
- 190 [14] J. J. Rohr and F. E. Fish, "Strouhal numbers and optimization of swimming by odontocete
191 cetaceans," *Journal of Experimental Biology*, vol. 207, pp. 1633–1642, Apr. 2004.
- 192 [15] G. K. Taylor, R. L. Nudds, and A. L. R. Thomas, "Flying and swimming animals cruise at a
193 Strouhal number tuned for high power efficiency," *Nature*, vol. 425, pp. 707–711, Oct. 2003.
- 194 [16] F. Fish, "Advantages of natural propulsive systems," *Marine Technology Society Journal*, vol. 47,
195 pp. 37–44, 09 2013.

- 196 [17] R. W. Blake, "The Mechanics of Labriform Locomotion: I. Labriform Locomotion in the
197 Angelfish (*Pterophyllum Eimekei*): an Analysis of the Power Stroke," *Journal of Experimental*
198 *Biology*, vol. 82, pp. 255–271, Oct. 1979.
- 199 [18] X. Tong and C. Tang, "Design of a monitoring system for robotic fish in underwater environment,"
200 *International Journal of Vehicle Information and Communication Systems*, vol. 3, no. 4, pp. 321–
201 335, 2018.
- 202 [19] J. Wang, *Robotic fish: Development, modeling, and application to mobile sensing*. Michigan
203 State University, 2014.
- 204 [20] K. Sampath, J. D. Geder, R. Ramamurti, M. D. Pruessner, and R. Koehler, "Hydrodynamics of
205 tandem flapping pectoral fins with varying stroke phase offsets," *Physical Review Fluids*, vol. 5,
206 p. 094101, Sept. 2020. Publisher: American Physical Society.
- 207 [21] A. P. Mignano, S. Kadapa, J. L. Tangorra, and G. V. Lauder, "Passing the Wake: Using Multiple
208 Fins to Shape Forces for Swimming," *Biomimetics*, vol. 4, p. 23, Mar. 2019. Number: 1
209 Publisher: Multidisciplinary Digital Publishing Institute.
- 210 [22] A.-T. Nedelcu, C. Faităr, L.-C. Stan, and N. Buzbuchi, "Underwater Vehicle CFD Analyses and
211 Reusable Energy Inspired by Biomimetic Approach," preprint, ENGINEERING, Aug. 2018.
- 212 [23] J. L. Tangorra, S. N. Davidson, I. W. Hunter, P. G. A. Madden, G. V. Lauder, H. Dong,
213 M. Bozkurttas, and R. Mittal, "The Development of a Biologically Inspired Propulsor for
214 Unmanned Underwater Vehicles," *IEEE Journal of Oceanic Engineering*, vol. 32, pp. 533–550,
215 July 2007.
- 216 [24] G. V. Lauder and P. G. A. Madden, "Learning from fish: Kinematics and experimental hy-
217 drodynamics for roboticists," *International Journal of Automation and Computing*, vol. 3,
218 pp. 325–335, Oct. 2006.
- 219 [25] H. Vardhan, P. Volgyesi, W. Hedgecock, and J. Sztipanovits, "Constrained Bayesian Optimiza-
220 tion for Automatic Underwater Vehicle Hull Design," in *Proceedings of Cyber-Physical Systems*
221 and *Internet of Things Week 2023, CPS-IoT Week '23*, (New York, NY, USA), pp. 116–121,
222 Association for Computing Machinery, May 2023.
- 223 [26] K. Sampath, N. Xu, J. Geder, M. Pruessner, and R. Ramamurti, "Flapping Soft Fin Defor-
224 mation Modeling using Planar Laser-Induced Fluorescence Imaging," *Journal of Visualized*
225 *Experiments*, p. 63784, Apr. 2022.
- 226 [27] J. S. Palmisano, J. D. Geder, M. D. Pruessner, and R. Ramamurti, "Power and Thrust Comparison
227 of Bio-mimetic Pectoral Fins with Traditional Propeller-based Thrusters," in *18th International*
228 *Symposium on Unmanned Untethered Submersible Technology*, p. 8, 2013.
- 229 [28] K. Viswanath, A. Sharma, S. Gabbita, J. Geder, R. Ramamurti, and M. Pruessner, "Evaluation
230 of surrogate models for multi-fin flapping propulsion systems," in *OCEANS 2019 MTS/IEEE*
231 *SEATTLE*, pp. 1–9, 2019.
- 232 [29] J. Lee, K. Viswanath, A. Sharma, J. Geder, R. Ramamurti, and M. D. Pruessner, "Data-Driven
233 Approaches for Thrust Prediction in Underwater Flapping Fin Propulsion Systems," p. 8, 2021.
- 234 [30] S. Bi, C. Niu, Y. Cai, L. Zhang, and H. Zhang, "A waypoint-tracking controller for a bionic
235 autonomous underwater vehicle with two pectoral fins," *Advanced Robotics*, vol. 28, 02 2014.
- 236 [31] Y. Shan, Y. Bayiz, and B. Cheng, "Efficient thrust generation in robotic fish caudal fins using
237 policy search," *IET Cyber-systems and Robotics*, vol. 1, pp. 38–44, June 2019. Publisher
238 Copyright: © 2021 Zhejiang University Press.
- 239 [32] P. Stankiewicz, Y. T. Tan, and M. Kobilarov, "Adaptive sampling with an autonomous underwater
240 vehicle in static marine environments," *Journal of Field Robotics*, vol. 38, no. 4, pp. 572–597,
241 2021. _eprint: <https://onlinelibrary.wiley.com/doi/pdf/10.1002/rob.22005>.
- 242 [33] H. Zhou, J. J. Gómez-Hernández, and L. Li, "A pattern-search-based inverse method," *Water*
243 *Resources Research*, vol. 48, no. 3, 2012.

- 244 [34] T. M. Hansen and K. S. Cordua, "Efficient Monte Carlo sampling of inverse prob-
 245 lems using a neural network-based forward—applied to GPR crosshole traveltime inver-
 246 sion," *Geophysical Journal International*, vol. 211, pp. 1524–1533, Sept. 2017. _eprint:
 247 <https://academic.oup.com/gji/article-pdf/211/3/1524/27761026/ggx380.pdf>.
- 248 [35] K. El Hamidi, M. Mjahed, A. El Kari, and H. Ayad, "Adaptive control using neural networks and
 249 approximate models for nonlinear dynamic systems," *Modelling and Simulation in Engineering*,
 250 vol. 2020, no. 1, p. 8642915, 2020.
- 251 [36] B. Wehbe, M. Hildebrandt, and F. Kirchner, "A Framework for On-line Learning of Underwater
 252 Vehicles Dynamic Models," in *2019 International Conference on Robotics and Automation*
 253 (*ICRA*), (Montreal, QC, Canada), pp. 7969–7975, IEEE, May 2019.
- 254 [37] J. Muliadi and B. Kusumoputro, "Neural network control system of uav altitude dynamics and
 255 its comparison with the pid control system," *Journal of Advanced Transportation*, vol. 2018,
 256 no. 1, p. 3823201, 2018.
- 257 [38] C. McGann, F. Py, K. Rajan, J. Ryan, and R. Henthorn, "Adaptive Control for Autonomous
 258 Underwater Vehicles," in *Proceedings of the Twenty-Third AAAI Conference on Artificial*
 259 *Intelligence*, AAAI, 2008.
- 260 [39] V. Torczon, "On the Convergence of Pattern Search Algorithms," *SIAM Journal on Optimization*,
 261 vol. 7, no. 1, pp. 1–25, 1997.
- 262 [40] J. D. Geder, J. Palmisano, R. Ramamurti, W. C. Sandberg, and B. Ratna, "Fuzzy logic pid based
 263 control design and performance for a pectoral fin propelled unmanned underwater vehicle," in
 264 *2008 International Conference on Control, Automation and Systems*, pp. 40–46, 2008.
- 265 [41] B. Zhou, J. Geder, A. Sharma, J. Lee, M. Pruessner, R. Ramamurti, and K. Viswanath, "Compu-
 266 tational approaches for modeling power consumption on an underwater flapping fin propulsion
 267 system," 2023.
- 268 [42] J. D. Geder, R. Ramamurti, K. Sampath, M. Pruessner, and K. Viswanath, "Fluid-Structure
 269 Modeling and the Effects of Passively Deforming Fins in Flapping Propulsion Systems," in
 270 *OCEANS 2021: San Diego – Porto*, pp. 1–9, Sept. 2021. ISSN: 0197-7385.
- 271 [43] J. Dabney and T. Harman, "Mastering simulink," 01 1998.
- 272 [44] D. Kroese, T. Brereton, T. Taimre, and Z. Botev, "Why the Monte Carlo method is so important
 273 today," *Wiley Interdisciplinary Reviews: Computational Statistics*, vol. 6, 11 2014.
- 274 [45] C. Audet, "A Survey on Direct Search Methods for Blackbox Optimization and Their Applica-
 275 tions," *Mathematics Without Boundaries: Surveys in Interdisciplinary Research*, pp. 31–56, 04
 276 2014.
- 277 [46] R. Hooke and T. A. Jeeves, "'Direct Search' Solution of Numerical and Statistical Problems,"
 278 *Journal of the ACM*, vol. 8, pp. 212–229, Apr. 1961.
- 279 [47] B. Zhou, J. Geder, K. Viswanath, A. Sharma, and J. Lee, "Power-aware inverse-search ma-
 280 chine learning for low resource multi-objective unmanned underwater vehicle control (student
 281 abstract)," *Proceedings of the AAAI Conference on Artificial Intelligence*, vol. 38, pp. 23714–
 282 23716, Mar. 2024.